Int J Adv Manuf Technol (2017) 90:1419–1432
DOI 10.1007/s00170-016-9403-9

ORIGINAL ARTICLE

Parameters optimization and objective trend analysis for fiber laser keyhole welding based on Taguchi-FEA

Yuewei Ai[1] · **Jianzhuang Wang**[1] · **Ping Jiang**[1] · **Yang Liu**[1] · **Wei Liu**[1]

Received: 2 March 2016 / Accepted: 29 August 2016 / Published online: 23 September 2016

Abstract This paper proposes an integrated method for process parameters optimization and objective analysis in the fiber laser keyhole welding based on Taguchi and finite element method (FEA). The Taguchi-FEA framework is established and applied for the objective of increasing the ratio of weld penetration to width (P/W) in the welded joints. Numerical simulations are incorporated into identifying the desired responses and the process parameters effects on the objective without consuming time, materials, and labor effort. To validate the effectiveness of the integration methodology, the fiber laser keyhole welding of the hot-dip galvanized dual phase sheet (GA-DP590) has been carried out in this paper. The three process parameters, laser power (LP), welding speed (WS), and focal position (FP), have been taken into consideration during the optimization process. The optimized results are confirmed, and trend of the objective variation near the optimal process parameters is analyzed by the numerical simulation. The corresponding microstructure, phase transformation and microhardness variation of the optimized weld bead are also calculated. The results demonstrate that the proposed method is reliable and effective for improving the quality of welded joints in the practical production level.

Keywords Welding simulation · Taguchi · Fiber laser · Optimization

✉ Ping Jiang
jiangping@mail.hust.edu.cn

[1] The State Key Laboratory of Digital Manufacturing Equipment and Technology, School of Mechanical Science and Engineering, Huazhong University of Science & Technology, 430074 Wuhan, People's Republic of China

Abbreviations

HAZ	Heat-affected zone
LP	Laser power
WS	Welding speed
FP	Focal position
DOE	Design of experiments
P/W	Weld penetration to width
GA	Genetic algorithm
RSM	Response surface methodology
FEA	Finite element analysis
S/N	Signal to noise
ANOVA	Analysis of variance
BM	Base materials
Dof	Degrees of freedom
PV	Predicted value
FZ	Fusion zone
M	Martensite
A	Austenite
FAG	Fine equiaxed grains

1 Introduction

Laser welding has been widely used in a variety of industrial applications due to the offering advantages of high power intensity, high productivity, high penetration, and narrow heat-affected zone (HAZ). The irradiated materials will be evaporated from the surface of molten pool when the laser intensity is above the critical limit. The keyhole mode welding is correspondingly achieved, and the vapor and plasma are formed. The high dynamic welding process comprises complex multidimensional mechanisms, which makes it difficult to fully control the process and anticipate welded joints defects. During the fiber laser keyhole welding process, the incomplete fusion, porosity, humping, and other welding defects

are easily generated with adopting the inappropriate process parameters [1]. The quality of welded joints can be defined in terms of properties such as weld bead geometry, mechanical properties, and distortion [2, 3]. It is observed that the process parameters like laser power (LP), welding speed (WS), and focal position (FP) play a significant role in determining the weld bead geometry and hence the welding quality. Casalino et al. [4] discussed the influence of different welding conditions on the weld bead morphology and mechanical properties. Zhang et al. [5] studied the effects of welding process parameters on hot cracking and fusion ratio of welded joints. Therefore, how to select the proper process parameters for high quality welded joints has become a very important challenge.

The relationship between the process parameters and welding bead geometry is non-liner and complicated. The extent of contribution of the actual process parameters towards the results is particularly difficult to be identified. It is always a puzzling problem which causes operators can only select the welding process condition according to experience, charts, and handbooks in the practical production [6–8]. The process parameters determined by trial and error method may yield fairly good results, but it is hard to ensure achieving the optimal weld bead, especially not applicable for the new welding process. To obtain the desired weld bead without consuming time, materials, and labor effort, there are various reports about the mathematical model used to optimize the process parameters through correlating input variables with output responses. The design of experiments (DOE) and statistical method are widely used in the welding field. Tarng et al. [9] adopted the Taguchi method to obtain the setting of optimal welding process parameters. The application of Taguchi method in finding of the combination of the major welding control factors to produce low level defects was investigated by Casalino et al. [10]. Datta et al. [11] used the Taguchi philosophy for exploring the optimal parametric combinations to achieve desired weld bead geometry and dimensions related to the HAZ. Taguchi addresses quality in two main areas: off-line and online quality control [12]. Compared with the classical experimental design, the most important difference is that the Taguchi method-based robust design technique considers the minimization of the variance of the characteristic of interest. Although, the Taguchi method has drawn much criticism due to several major limitations like difficulties in modeling, time-consuming, and cumbersome, it has been able to solve single response problems effectively [13]. Therefore, it is very useful to model the fiber laser keyhole welding process using Taguchi technique with the objective of the maximum of the ratio of weld penetration to width (P/W).

Additionally, most of these optimization methods are usually taken to obtain the near-optimal parameters in the welding process. Correia et al. [14] studied the implementation possibility of using genetic algorithm (GA) as a method to decide near-optimal settings of GMAW process. Winiczenko [15] investigated a hybrid response surface methodology (RSM) and GA-based technique for determining the near-optimal settings in the friction welding process parameters. However, the optimal results were still required validation by costly and time-consuming experimental approaches. Moreover, some of the optimal solution validations are impossible due to the limitation of current process conditions. Thus, the optimal process parameters are not confirmed directly by the optimal solution which is often replaced by the near-optimal settings of the process parameters. These approximate treatments are not accurate and acceptable, because to some extent that the response is frequently mutational near the optimal settings. Fortunately, numerical simulations of welding process provide a promising way for this regard. For several decades, finite element analysis (FEA) has become a powerful tool and been widely used in simulating the temperature field behavior during laser welding process. There are a large number of researchers used FEA for welding simulation successfully, especially for weld shape prediction. The initial welding simulations were simplified certainly base on moving line source and surface source [16]. Although the line source and surface source could indicate the ranges of temperature and welding conditions, the results were different from those found experimentally. Belhadia et al. [17] studied the combined heat source of Gaussian surface source and cylindrical volume source to investigate the weld bead shape. It showed that the combined heat source was essential in predicting weld bead. Wang et al. [18] developed a combined volume heat source model consisting of a rotary Gaussian heat source and a double ellipsoid heat source for the simulation of weld shape prediction during laser keyhole welding process. Franco et al. [19] proposed a double source of a semi-infinite solid and an infinite one for predicting seam geometry in laser beam welding of

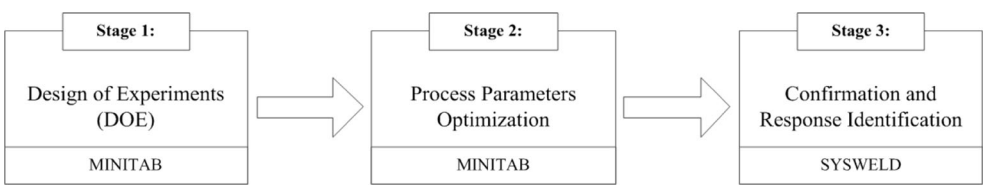

Fig. 1 The framework of Taguchi-FEA

stainless steel. It is evident that FEA is a very useful tool for welding process simulation. However, FEA of welding simulating has not been used to replace the expensive experiments to validate the optimal results obtained from the mathematical model optimization. Moreover, the objective variation trend near the optimal settings and the microstructure, phase transformation and microhardness profile has not been analyzed by FEA, which causes that the optimal results are not validated fully.

In this paper, a Taguchi-FEA integrated method is proposed for process parameters optimization and objective trend analysis in fiber laser keyhole welding. Firstly, Taguchi L_{25} orthogonal array is used for optimizing process parameters in the fiber keyhole laser welding of hot-dip galvanized dual phase sheet (GA-DP590). Three process parameters namely LP, WS, and FP have been optimized to maximize the P/W ratio. The optimum levels of process parameters have been identified based on the signal to noise (S/N) ratio. The analysis of variance (ANOVA) is used to compare the impact of process parameters on the weld bead P/W ratio and determine the most significant factors. Then, a 3D weld bead predicted model of FEA is established and validated by experimental results. The near-optimal settings obtained from the statistical techniques, Taguchi method, are confirmed by FEA and experiments, respectively. Simultaneously, the objective variation trend near the optimal settings and microstructure, phase transformation and microhardness variation of the weld bead from the optimal conditions are identified through the welding numerical simulation.

The structure of this paper is organized as follows. In section 2, the general framework of the proposed Taguchi-FEA integrated optimization method is introduced. In section 3, DOE and process parameters optimization by Taguchi techniques are discussed. In section 4, weld bead predicting model of FEA based on hybrid heat source and welding simulation validation have been described. In section 5, the optimized results are confirmed by weld simulation and experiments, and the trend analysis of the objective variation near the optimal settings, microstructure, phase transformation, and microhardness variation are conducted. Finally, the conclusions of the current study are offered.

2 General framework of integration method

The proposed Taguchi-FEA method is based on three subsequently implemented stages as shown in Fig. 1. The first stage includes DOE and experiments implementation. The DOE is done by Taguchi in the statistical software, MINITAB16. During the analysis, the LP, WS, and FP three welding process parameters are considered as design variables. The P/W ratio

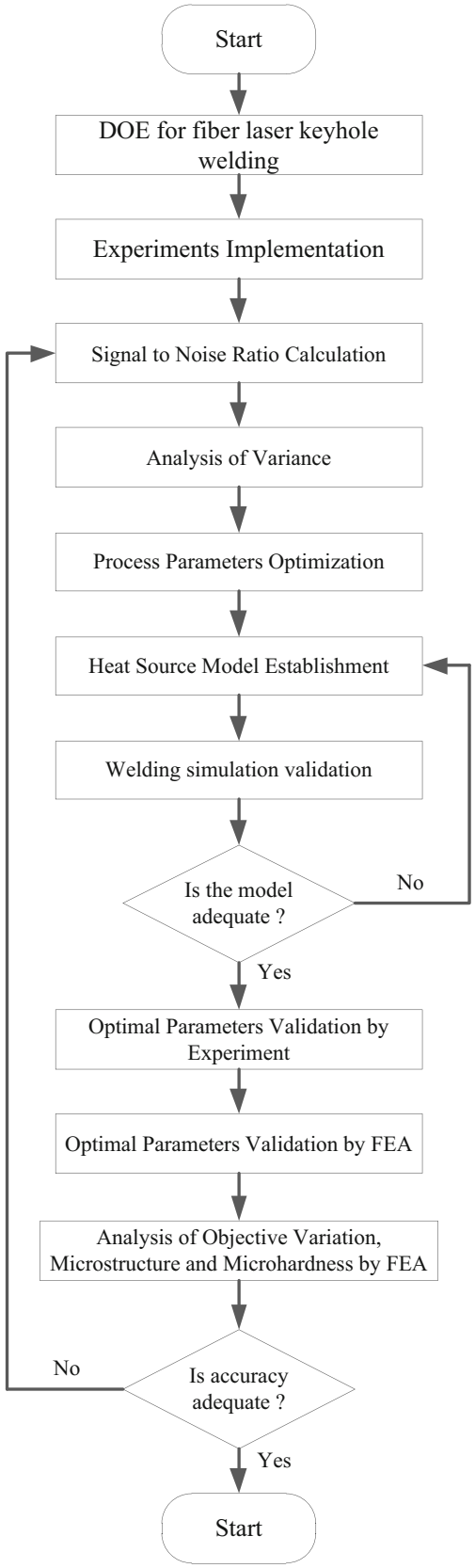

Fig. 2 The flowchart of Taguchi-FEA

Table 1 Chemical composition of the base material (Wt%)

Materials	C	Si	Mn	P	S	Al	B	Cr	Mo	Nb	Ti	Ni	Fe
GA-DP590	0.051	0.015	1.51	0.012	0.005	0.033	0.00005	0.031	0.025	0.011	0.0008	0.02	Bal.

is as the optimal objective. The whole process is converted into a three inputs and one output problem. Then, the Taguchi matrix is generated. According to the designed matrix, the experiments are carried out and the results are recorded. GA-DP590 is selected as the experimental material, and the welding system in this study is the fiber laser welding system.

The second stage is focused on the welding process parameters optimization. MINITAB16 is used as the optimization tool. Based on the S/N ratio, the optimum levels of process parameters are determined. The significant contributions of parameters are identified by the ANOVA. The objective investigated in the current research is to maximize the P/W ratio of the weld bead. During this stage, the larger the better S/N ratio is calculated. The process parameters effects on the response are identified in the ANOVA.

The third stage is experiment and FEA confirmation and the identification of the response of process parameters near the optimal settings. The whole process consists of the following four steps:

- Hybrid heat source model establishment for the fiber laser keyhole welding.
- Welding simulation validation based on the proposed hybrid heat source model.
- The experimental validation of optimal process parameters.
- The near-optimal settings confirmation and response identification by using FEA.

The hybrid heat source model of double ellipsoid heat source model and 3D Gaussian heat source is used for the fiber laser keyhole welding. Then, the numerical simulation of welding process is implemented based on the proposed heat source model, and the weld bead prediction is validated by the experiments. After welding simulation, the optimized results are confirmed by the experiments and FEA. To further confirm the optimal results, the trend analysis of the objective variation is conducted through identifying the response of process parameters near the optimal settings using FEA. Therefore, the effectiveness of the integrated methodology for welding process parameters optimization is verified fully. The overall optimization process based on Taguchi-FEA integrated method is illustrated in Fig. 2. Details of each stage are described in the following sections of this paper.

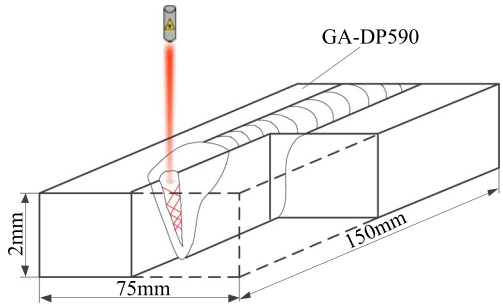

Fig. 3 Schematic of welding process

3 Experimental procedure

3.1 Materials

In the experiments, GA-DP590 was used as the base materials (BM) for the fiber laser keyhole welding. The composition of the GA-DP590 is presented in Table 1. They were cut into small plates as the welding specimens and the dimensions were 150 × 75 × 2 mm^3 as shown in Fig. 3. To protect the weld bead from disturbing with oil pollution and oxide film, the surface of specimens were cleaned by acetone.

3.2 Fiber laser keyhole welding

The welding system in this study is fiber laser welding system as shown in Fig. 4. The fiber laser, IPG YLR-

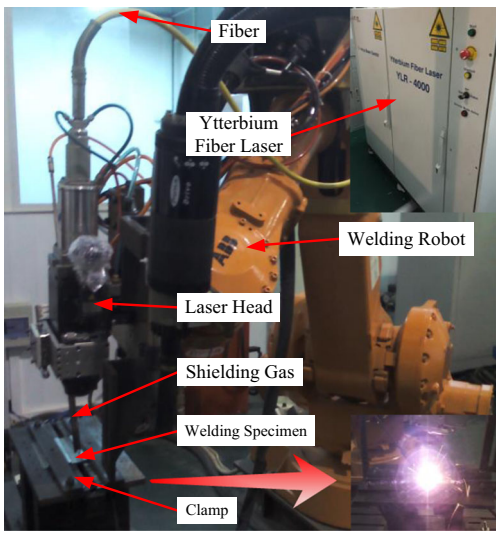

Fig. 4 The fiber laser welding system

Table 2 Welding parameters levels and response factor

Parameter	Unit	Notation	Factor levels				
			1	2	3	4	5
Laser power	W	LP	1500	2000	2500	3000	3500
Welding speed	m/min	WS	2.50	2.75	3.00	3.25	3.50
Focal position	mm	FP	−3.0	-1.5	0.0	1.5	3.0
Response factor							
P/W ratio	The ratio of weld penetration to width						

Table 4 Response table for means

Level	LP(W)	WS(m/min)	FP(mm)
1	0.8546	**1.2888**	1.162
2	1.0086	1.2416	**1.2868**
3	**1.3878**	1.1844	1.1736
4	1.2706	1.1272	1.2106
5	1.3362	1.0158	1.0248
Delta	0.5332	0.273	0.262
Rank	1	2	3

The optimal parameters based on mean are $LP_3WS_1FP_2$

4000, is with a wavelength of 1.06 um, and the diameter of optical fiber core is 0.3 mm. In the whole welding process, continuous wave fiber laser was used. The welding head was equipped with coaxial air blow protection device and grasped on the welding robot, ABB IRC5 M2004. The controlling system was used to set the welding process parameters, LP, WS, and FP included. During the welding process, the side blow argon shielding gas was supplied at a flow rate of 30 L/min.

3.3 Design of experiments

The P/W ratio affected by the main process parameter factors, LP, WS, and FP, were considered in this investigation. Every factor was divided into five levels with equal interval. The present problem was converted into three factors and five level problem. The welding parameters levels and response factor were listed in Table 2. The total degrees of freedom (Dof) was

Table 3 Taguchi L_{25} design matrix and experimental results

No.	LP(W)	WS (m/min)	FP (mm)	P/W ratio	S/N ratio	Soundness of the bead
1	1500	2.5	−3	1.164	1.31906	Incomplete-penetration weld
2	1500	2.75	−1.5	1.058	0.48971	Incomplete-penetration weld
3	1500	3	0	0.673	−3.43970	Incomplete-penetration weld
4	1500	3.25	1.5	0.852	−1.39121	Incomplete-penetration weld
5	1500	3.5	3	0.526	−5.58029	Incomplete-penetration weld
6	2000	2.5	−1.5	1.489	3.45789	Penetration weld
7	2000	2.75	0	1.229	1.79104	Incomplete-penetration weld
8	2000	3	1.5	1.172	1.37855	Incomplete-penetration weld
9	2000	3.25	3	0.579	−4.74643	Incomplete-penetration weld
10	2000	3.5	−3	0.574	−4.82176	Incomplete-penetration weld
11	2500	2.5	0	1.274	2.10339	Penetration weld
12	2500	2.75	1.5	1.337	2.52263	Penetration weld
13	2500	3	3	1.493	3.48120	Penetration weld
14	2500	3.25	−3	1.560	3.86249	Penetration weld
15	2500	3.5	−1.5	1.275	2.11020	Incomplete-penetration weld
16	3000	2.5	1.5	1.286	2.18482	Penetration weld
17	3000	2.75	3	1.295	2.24540	Penetration weld
18	3000	3	−3	1.223	1.74853	Penetration weld
19	3000	3.25	−1.5	1.251	1.94515	Penetration weld
20	3000	3.5	0	1.298	2.26549	Penetration weld
21	3500	2.5	3	1.231	1.80516	Penetration weld
22	3500	2.75	−3	1.289	2.20506	Penetration weld
23	3500	3	−1.5	1.361	2.67716	Penetration weld
24	3500	3.25	0	1.394	2.88526	Penetration weld
25	3500	3.5	1.5	1.406	2.95971	Penetration weld

Table 5 Response table for signal to noise ratios

Level	LP(W)	WS(m/min)	FP(mm)
1	−1.7205	**2.1741**	0.8627
2	−0.5881	1.8508	**2.136**
3	**2.816**	1.1691	1.1211
4	2.0779	0.5111	1.5309
5	2.5065	−0.6133	−0.559
Delta	4.5365	2.7874	2.695
Rank	1	2	3

The optimal parameters based on S/N ratios are $LP_3WS_1FP_2$

12. The designed Taguchi orthogonal array was L_{25} as shown in Table 3. It is suitable for the study because the Dof of the orthogonal array is greater than the total Dof of the factors.

3.4 The results of experiments

The experiments were conducted according to the designed L_{25}. To obtain the clear metallographic figures under the optical microscope, the small patches ($15 \times 15 \times 2$ mm^3) were cut from the welding area, polished, and corroded as the metallographic specimens. The weld penetration and width were measured by optical microscope. The measured results of the weld bead were presented in Table 3. From the Table 3, it is seen that more than half of the welding experiments are the penetration welding.

4 Process parameter optimization

4.1 Signal to noise ratio

The calculation of the S/N ratio is based on the quality of intended characteristics. From the calculated corresponding responses, the optimal level settings can be obtained. There are three calculating formulas given below [20–24].

Larger the better:

$$\mathrm{S/N\ ratio}(\eta) = -10\log_{10}\left(\frac{1}{n}\sum_{i=1}^{n}\frac{1}{y_i^2}\right) \quad (1)$$

where n is the number of replications. y_i is the response value, and $i = 1, 2,\ldots, n$. The larger the better is used for the problem where the quality characteristic of interest is to be maximized. This type of problem is regarded as the larger the better.

Smaller the better:

$$\mathrm{S/N\ ratio}(\eta) = -10\log_{10}\left(\frac{1}{n}\sum_{i=1}^{n}y_i^2\right) \quad (2)$$

This is defined as the smaller the better problem which is to obtain the minimization of the characteristic.

Nominal the best:

$$\mathrm{S/N\ ratio}(\eta) = -10\log_{10}\left(\frac{\mu^2}{\sigma^2}\right) \quad (3)$$

where

$$\mu^2 = \frac{y_1 + y_2 + y_3 + \cdots + y_n}{n};\ \ \sigma^2 = \frac{(y_i - \bar{y})^2}{n-1}$$

This is the nominal the best type of problem which intends to minimize the mean squared error around a specific target value.

The maximization of the P/W ratio is set as the objective in the current study. Therefore, the larger the better for S/N ratio is calculated, as shown in Table 3. The influences of the fiber laser keyhole welding parameters, LP, WS, and FP, are studied on the weld bead P/W ratio. The average mean and S/N ratio values of all levels are given in Tables 4 and 5. As the larger S/N ratio to the better quality characteristics, the optimal level of the process parameters is set as $LP_3WS_1FP_2$.

4.2 Analysis of variance

The main purpose of ANOVA is to adopt the statistical method to identify the significant factors for the objective, the P/W ratio. The analysis results from the ANOVA can reveal clearly how far the welding process parameter affects the response and the significant level of the considered factors. The results of the ANOVA for mean and S/N ratio are tabulated in Tables 6 and 7. The main effects for mean and S/N ratio are plotted in Figs. 5 and 6. The F and P tests are used to identify the significance of the welding process parameters. The high

Table 6 Analysis of variance for means of P/W ratio

Source	Dof	Seq SS	Adj SS	Adj MS	F	P	% contribution
LP(W)	4	1.0535	1.0535	0.26337	4.9	0.014	50.0142
WS(m/min)	4	0.2252	0.2252	0.05631	1.05	0.424	10.6912
FP(mm)	4	0.1822	0.1822	0.04555	0.85	0.522	8.6498
Residual error	12	0.6455	0.6455	0.05379			30.6447
Total	24	2.1064					100

Table 7 Analysis of variance for signal to noise ratios of P/W ratio

Source	Dof	Seq SS	Adj SS	Adj MS	F	P	% contribution
LP(W)	4	83.25	83.25	20.813	4.81	0.015	46.1884
WS(m/min)	4	24.86	24.86	6.214	1.44	0.282	13.7927
FP(mm)	4	20.17	20.17	5.043	1.16	0.374	11.1906
Residual error	12	51.96	51.96	4.33			28.8282
Total	24	180.24					100

Dof degrees of freedom, *Seq SS* sequential sum of squares, *Adj SS* adjusted sum of square, *Adj MS* adjusted mean square, *F* Fisher ratio, *P* probability

F value and the low *P* value demonstrate that the corresponding factor is the significant factor which plays an important role in affecting the response. From Tables 6 and 7 and Figs. 5 and 6, it is clearly seen that the LP is the most significant affecting factor for the P/W ratio. The WS and FP are the second and third affecting factors, respectively.

4.3 Predicted value of P/W ratio

According to the experiments, the optimal level of the process parameters is $LP_3WS_1FP_2$ which is evaluated from the literatures [13, 20]. The factor average values are taken from Table 4. The corresponding predicted value (PV) of P/W ratio is formulated as follows.

$$\begin{aligned} PV &= LP_3 + WS_1 + FP_2 - 2R_M \\ &= 1.388 + 1.289 + 1.287 - 2 \times 1.172 \\ &= 1.62 \end{aligned} \quad (4)$$

where LP_3 is the average mean value of LP at the third level. WS_1 is the average mean value of WS at the first level. FP_2 is the average mean value of FP at the second level. R_M is the overall mean.

5 Welding simulation confirmation and discussion

5.1 Heat source model

During the fiber laser keyhole welding, the complex energy distribution is hard to be simulated by a single heat source model. Ducharmer et al. [25] reported that total absorption of the laser energy is determined from detailed consideration of the inverse Bremsstrahlung absorption in the plasma and Fresnel absorption at the keyhole walls. However, the plasma is mainly distributed over the keyhole. Thus, the laser energy absorption is calculated as the inverse Bremsstrahlung absorption over the keyhole and Fresnel absorption in the inside of the keyhole, which requires a combined heat source model to describe the whole laser energy absorption [26]. In this paper, the popular double ellipsoid heat source model [27, 28] is adopted to simulate the inverse Bremsstrahlung absorption. It is a non-axisymmetric heat source which consists of two different ellipses, i.e., the quadrant of one ellipsoid as the front half source and the quadrant of another ellipsoid as the rear half, as shown in Fig. 7.

The double ellipsoid heat source model can be expressed as follows:

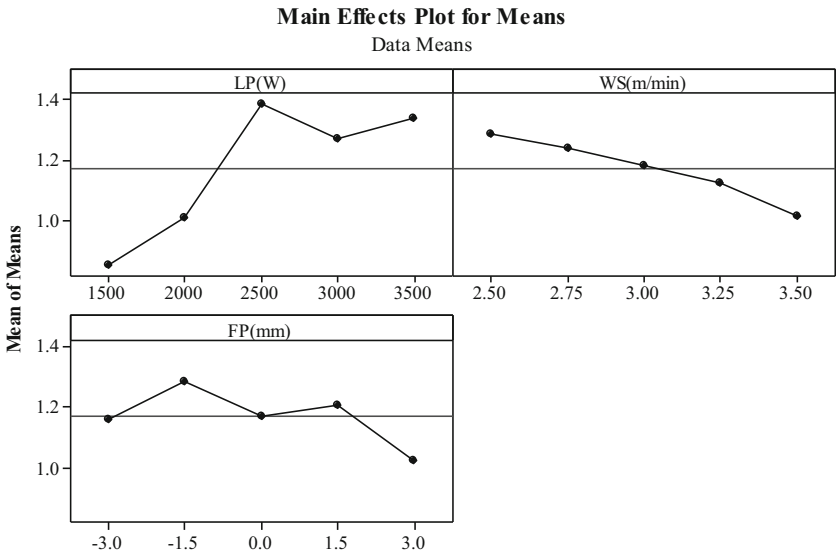

Fig. 5 Main effects plot for means of P/W ratio

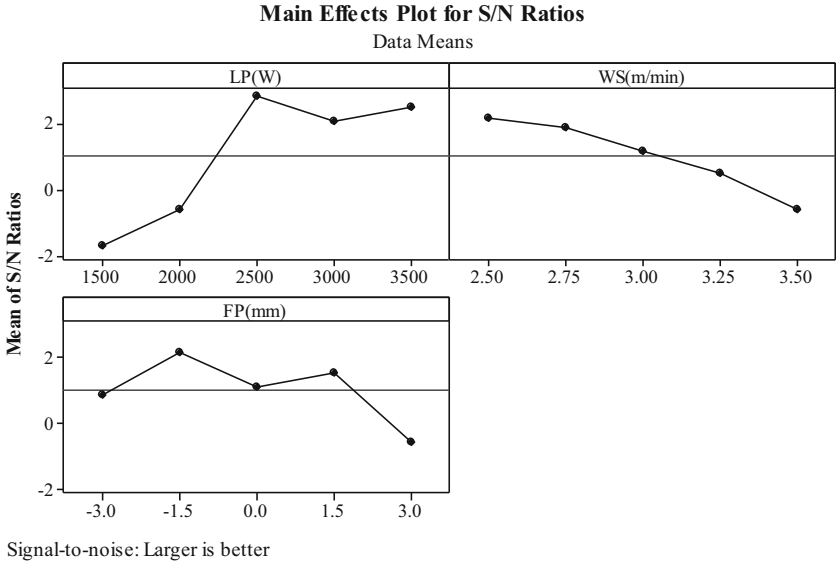

Fig. 6 Main effects plot for S/N ratios of P/W ratio

$$q_{\mathrm{f}}(x,y,z)=\frac{6\sqrt{3}f_{1}f_{\mathrm{f}}Q}{a_{\mathrm{f}}bc\pi\sqrt{\pi}}\exp\left(-3\left(\frac{x^2}{a_{\mathrm{f}}}+\frac{y^2}{b}+\frac{z^2}{c}\right)\right) \quad (5)$$

$$q_{\mathrm{r}}(x,y,z)=\frac{6\sqrt{3}f_{1}f_{\mathrm{r}}Q}{a_{\mathrm{r}}bc\pi\sqrt{\pi}}\exp\left(-3\left(\frac{x^2}{a_{\mathrm{r}}}+\frac{y^2}{b}+\frac{z^2}{c}\right)\right) \quad (6)$$

$$Q=\eta P \quad (7)$$

where $q_{\mathrm{f}}(x,y,z)$ and $q_{\mathrm{r}}(x,y,z)$ are the power densities of the double ellipsoid heat source in the inside of the front and rear quadrants of the heat source. Q is the effectively absorbed power. f_{f} and f_{r} are the fractional factors of the heat source deposited in the front and rear quadrant, which can be determined by $f_{\mathrm{f}}+f_{\mathrm{r}}=2$. The constants, a_{f}, a_{r}, b, and c are heat source parameters that define the size and shape of the ellipses and hence the heat source distribution. η is the absorption coefficient, and P is the laser power.

The 3D Gaussian heat source model [29] is applied along the longitudinal axis of the heat source model to describe the Fresnel absorption, as shown in Fig. 8.

The 3D Gaussian heat source model can be expressed as follows:

$$Q_{\mathrm{G}}(x,y,z)=Qf_{2}\exp\left[-\frac{r^2}{r_0^2(z)}\right] \quad (8)$$

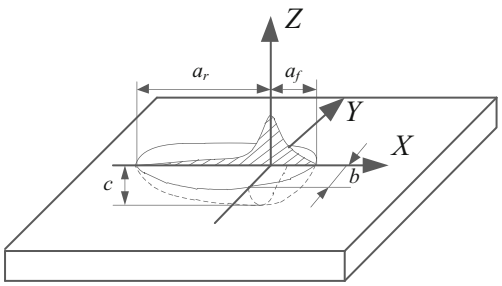

Fig. 7 Double ellipsoid heat source model

$$r^2=x^2+y^2 \quad (9)$$

$$r_0(z)=r_e-\frac{r_e-r_i}{z_e-z_i}(z_e-z) \quad (10)$$

where $Q_{\mathrm{G}}(x,y,z)$ is the power density of the 3D Gaussian heat source. f_1 and f_2 are the fractional factors of the heat deposited in double ellipsoid heat source and 3D Gaussian heat source, respectively. r is the distance away from the heat source center, the radius. r_{e} and z_{e} are the radius and height of the laser heat source in the upper plane. r_{i} and z_{i} are the radius and height of laser heat source in the lower plane.

5.2 Simulation model validation

The weld shape prediction of the fiber laser keyhole welding was carried out using the commercial FEA Software, SYSWELD. During the simulation process, the local refinement mesh model is used to improve

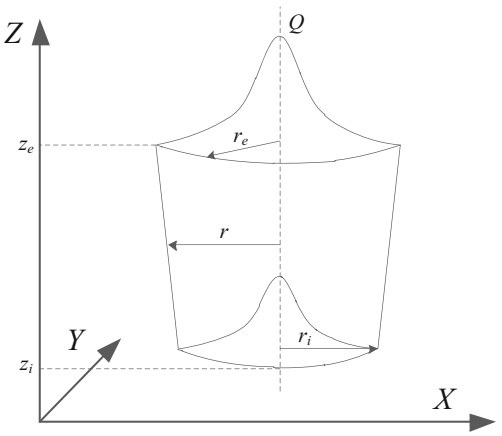

Fig. 8 3D Gaussian heat source model

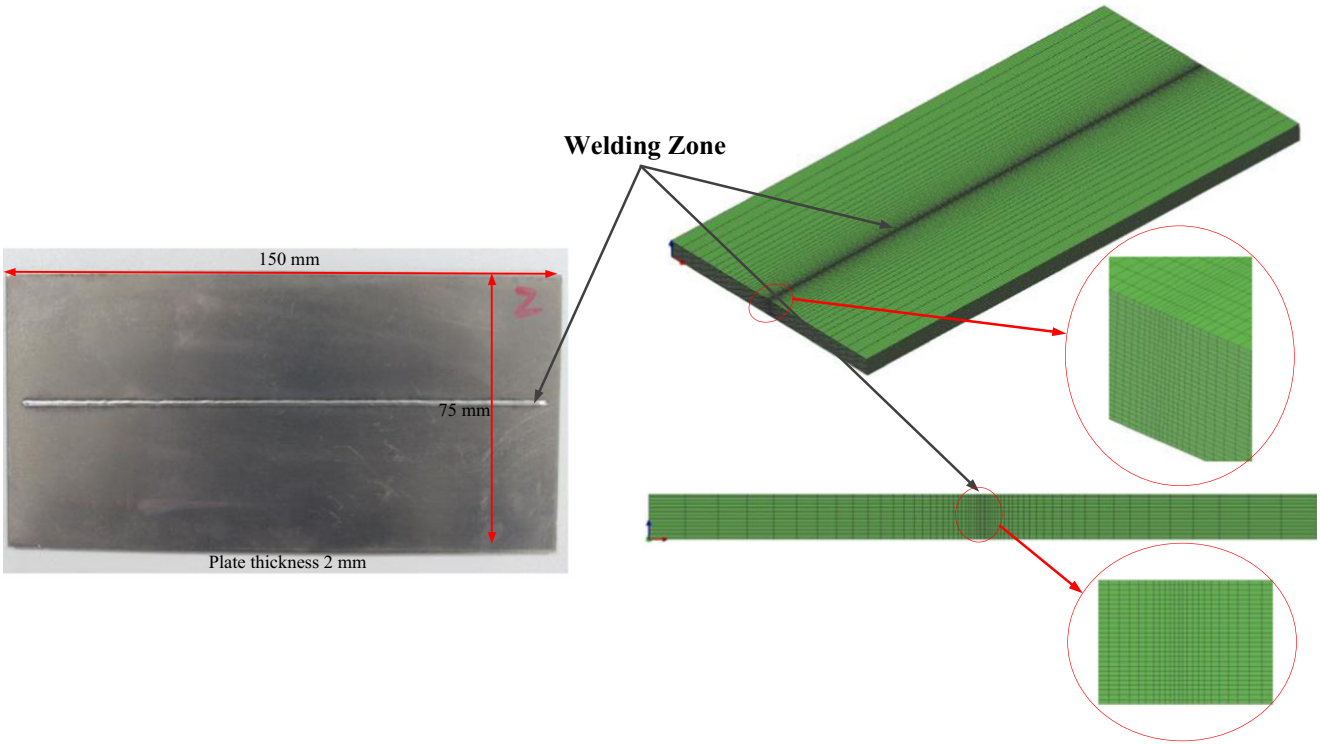

Fig. 9 Experimental model (*left*) and 3D FEA model (*right*) of fiber laser keyhole welding specimen

simulation accuracy while not considerably increasing the computational time. Actually, the welding zone around the heat source model is the focused area. The mesh in the welding zone is refined as the bell curve criterion and the scaling factor is equal to 25. The refined mesh model used in the welding simulation process is illustrated in Fig. 9.

The describing thermal source loading to the material represented by the Fortran time-space function fits the laser energy density distribution the best [29]. Heat losses caused by the convection, radiation, and contact are taken into considered by the corresponding thermal coefficients. The predictions of weld bead shape of fiber laser keyhole welding have been validated by experimental results. The temperature contour corresponds to the weld bead cross-section dimensions. The temperature of fusion zone (FZ) is higher than melting point (1420 °C). The predicted results were compared with the weld macrograph of experimental weld cross sections, and both of the weld bead boundary shape and size were found to be in good agreement, as shown in Fig. 10. The experimental weld bead is depicted in Fig. 10a with red line, and the corresponding predicted result of weld bead is shown in Fig. 10b by white line.

5.3 Results and discussion

5.3.1 Weld bead comparison

To verify the optimal results, the confirmation experiments were carried out. The process parameters were adopted as the optimum levels. The optimal process parameters are

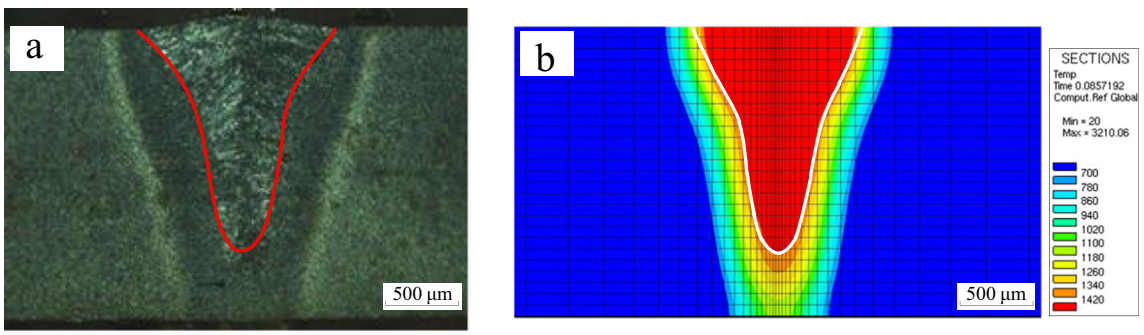

Fig. 10 Weld bead shape comparison: **a** experimental result; **b** simulation result (P = 2000 W, WS = 3.5 m/min, F = 0 mm)

Table 8 Confirmation test results

Algorithm	P/W ratio	LP(W)	WS(m/min)	FP(mm)
Taguchi optimal solution	1.620	2500	2.50	−1.50
Feasible solution	1.589	2500	2.50	−1.50
Feasible solution	1.591	2500	2.50	−1.50
Feasible solution	1.596	2500	2.50	−1.50
Average value	1.592	2500	2.50	−1.50
Error (%)	1.728	–	–	–

$LP_3WS_1FP_2$, LP 2500 W, WS 2.50 m/min, and FP −1.5 mm, respectively. During the optimized result confirmation, three groups of testing experiments were implemented. The average value of the P/W ratio from the three measured metallographic specimens in the fiber laser keyhole welded joints was 1.592, as shown in Table 8. Therefore, the optimized result is in good agreement with the experimental result, and the error is negligible.

5.3.2 Simulation confirmation and trend analysis of the objective variation

The optimal result was also confirmed by the FEA simulation in this study. From the simulation result, the predicted P/W ratio was 1.594 at the optimal level settings of process parameters. The results between the simulated and optimal keep almost consistent, as shown in Table 9. To further confirm the optimized value and improve the implementation possibility in the practical, trend analysis of the objective variation near-optimal settings of process parameters based on FEA simulation was carried out in this section. According to the ANOVA, the LP and WS are identified as the most significant affecting factors for the response, P/W ratio. In practical production, the LP and WS often fluctuate in a certain range, which is difficult to be controlled. Moreover, some optimal solution validations through experiments are impossible since the current process conditions are hard to meet the precision requirement. It is widely adopted that optimal process parameters are not confirmed directly and replaced by the near-optimal settings of the process parameters. Thus, the trend analysis of the objective near-optimal settings by FEA simulation is essential for improving the theoretical significance and engineering value of the optimization process. In the current research, the objective trend analysis on the LP and WS variation near the optimal settings of the process parameters was conducted, as presented in Tables 9 and 10. From the tables, it is obvious that the P/W ratio values with the near-optimal process parameters are all smaller than that in the optimal settings. It is clearly seen that the optimal results are found to be agreed with the simulation confirmation, which approves that the obtained results are the global optimized values other than the local optimized results.

Through the FEA simulation, the trend of the objective variation affected by individual process parameters has been illustrated in Fig. 11. To identify the effects of two significant process parameters in a single plot, the variables values are represented by the FEA number in the figures. From the Fig. 11, it is clear seen that the P/W ratio increases with the LP increase before 2500 W and then decreases. This is due to the fact that firstly with the increase of LP, the heat input also increases which leads to weld penetration increasing greatly, while the weld width only has slight increase. When the LP achieves the critical limit, the welding mode is converted to penetration weld, and the increased heat input mainly used to enlarge the weld width, which causes the P/W ratio gradually decreases. Furthermore, it is obvious that an increase in WS decreases the P/W ratio due to the heat input decreasing at a certain time. High WS often causes poor weld penetration resulting in the negative effect on weld bead geometry and mechanical properties. The analyzed result is kept in consistent with the practical welding process [30–32]. From the above discussion, FEA simulation is essential for objective variation analysis without consuming time, materials, and labor effort.

5.3.3 Microstructure evolution

The weld bead microstructures of GA-DP590 will be transformed when subjected to the thermal cycle of fiber laser keyhole welding. The thermal cycle curve of the optimal weld bead along the welding path in the quasi steady state during the welding process is shown in Fig. 12. It is clear that the peak temperature of the detecting node is 2400 °C when quasi steady state is achieved. The thermal cycle

Table 9 FEA validation on LP

FEA	1	2	3	4	5	6	7	8	9	10	11
LP(W)	2000	2100	2200	2300	2400	2500	2600	2700	2800	2900	3000
P/W ratio	1.210	1.361	1.494	1.574	1.585	1.594	1.545	1.500	1.476	1.442	1.423

When the WS is 2.5 m/min and the FP is −1.5 mm

Table 10 FEA validation on WS

FEA	1	2	3	4	5	6	7	8	9	10	11
WS(m/min)	2.5	2.6	2.7	2.8	2.9	3	3.1	3.2	3.3	3.4	3.5
P/W ratio	1.594	1.593	1.590	1.587	1.582	1.573	1.556	1.540	1.478	1.445	1.368

When the LP is 2500 W and the FP is −1.5 mm

curve illustrates the high heating rate and slow cooling rate. A relative slow cooling rate observed is duo to the heat supplied to the trailing side nodes from the advancing heat source [33, 34], which leads to a long melt pool.

A significant change in microstructure of the optimized weld bead can be seen from the cross section of the welded joints. The formation of FZ and HAZ which co-existed with the unaffected BM at both sides of the weld as indicated in Fig. 13a. The phase transformation curve of FZ is shown in Fig. 12. In the FZ, austenite (A) starts to form since the temperature rises quickly above Ac_1 line of the steel, and the weld pool is fully austenized when the temperature is above Ac_3 line. Due to the high WS (2.5 m/min), the temperature above Ac_3 is only lasted a short time and then starts to decrease. The rapid cooling austenite is subsequently transformed to form martensite (M) and the volume fraction of which increased as the temperature moved away from the Ac_3 line towards the Ac_1 line as can be seen in Fig. 12, only a small amount of A existing in the FZ. The simulated results are in good match with the experimental results, as shown in Fig. 13. Metallographic examination of weld bead denotes that the FZ is dominantly martensitic structure with a lathy morphology in conjunction with a small amount of A The equiaxed dendrites with variable direction distribution is observed in the region closing to the FZ/HAZ interface, as shown in Fig. 13b and d. There is a zone characterized by fine equiaxed grains (FAG) occurring at the HAZ, which

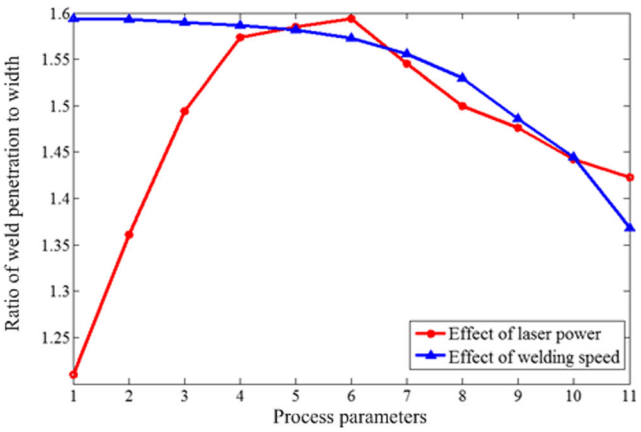

Fig. 11 Effects of LP and WS on the welding P/W ratio

is formed due to the constitutional undercooling. In the HAZ closing to the FZ, the undercooling is little, and epitaxial growth occurs from many nuclei as the same lattice structure of the BM grains. The HAZ microstructure contains ferrite, martensite, and bainite which formed as solid state transformation products of A From the microstructures of the welded joint from the optimal process parameters, there are no porosity, solidification cracks, and other micro defects. Therefore, this type of microstructure of the optimized weld bead is beneficial for quality improvement.

5.3.4 Microhardness profile

Numerical predictions of the microhardness profile were validated at the transverse cross section of the optimized welded specimens using a hardness tester (Qness) to obtain microshardness variations among the various welding regions. The Vickers microhardness values were measured (mid-section, 0.1 mm intervals in FZ and 0.2 mm intervals in other regions) under a 50 g load and 8 s dwell time. Figure 14 shows the simulated microhardness values taken at the central portion nodes of transverse cross section of the weld bead and plotted as a function of distance from the weld center line and compared with the measured values. The microhardness profile exhibited a symmetric characteristic with a lower BM hardness (~225 HV) followed by a sharp increase through the HAZ up into the FZ (~480 HV). The influencing factors of hardness increase in the FZ may result from the finer grains formation, formation of A structures, and other factors. However, the finer grains formation is negligible according to the above microstructure discussion (Figs. 12 and 13). The thermal cycle and phase transformation curves (Fig. 12) show that the high heating and cooling rate are associated with fiber laser keyhole welding, and it is very beneficial for the Mgrowth, which leads to highly increasing hardness values. Thus, the primary factor of the hardness changing in FZ region is the M formation. From hardness value changes, it also reveals that the width of weld bead is approximately 1.200 mm. It can be clearly seen a good agreement between the simulated and measured values. The small difference in the values may be due to experimental errors and assumptions made during numerical simulation.

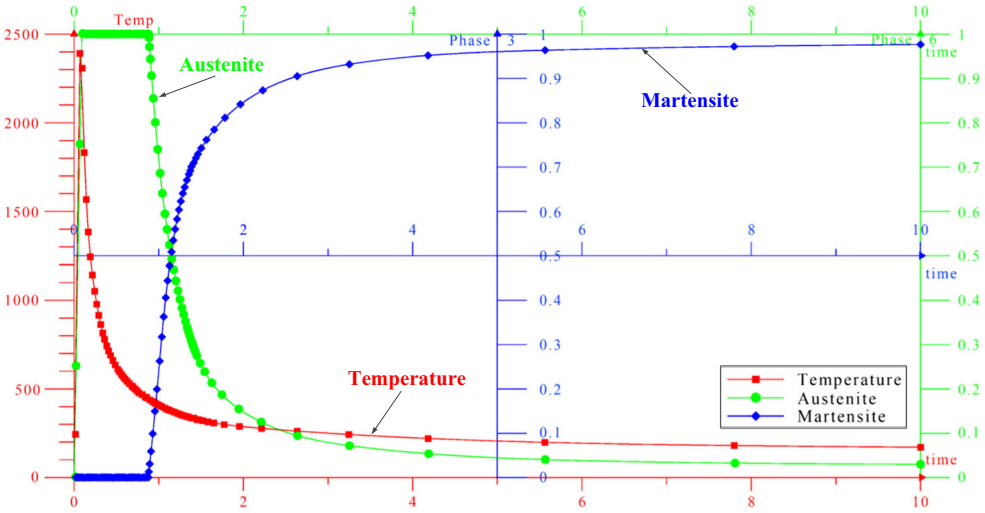

Fig. 12 The thermal cycle and phase transformation curves of the nodes in the FZ

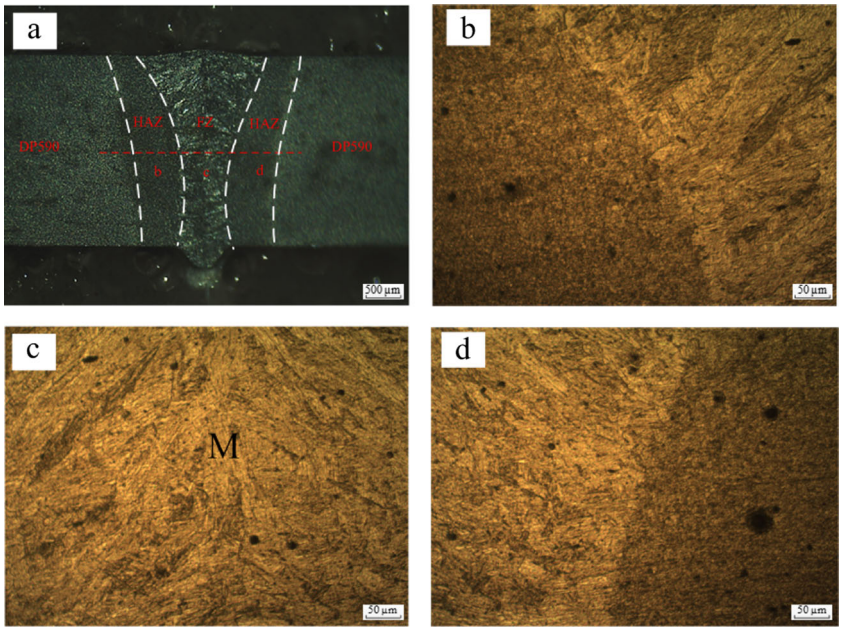

Fig. 13 **a**–**d** Microstructures of weld zone and interface between FZ and BM

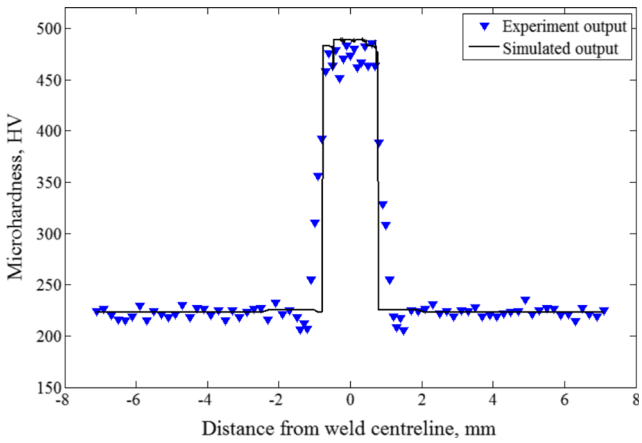

Fig. 14 Microhardness profile of the weld cross section

6 Conclusion

In this context, this paper proposed an integrated method of process parameters optimizing and objective analysis for the fiber laser keyhole welding using Taguchi technique and numerical simulation. The welding process parameters were optimized with the objective of maximum P/W ratio by Taguchi technique. The optimal values of the LP, WS, and FP are 2500 W, 2.5 m/min, and −1.5 mm, respectively, and the corresponding maximal P/W ratio is 1.620. Based on ANOVA, the LP and WS are identified as the most significant affecting factors for the response, P/W ratio. The optimized results are validated by experiments and FEA simulation. The results of optimal solution, experiments, and simulation were achieved

good agreement. Simultaneously, the trend of the objective variation near the optimal process parameters (LP and WS) and the microstructure, phase transformation and microhardness variation of the optimized weld bead are also analyzed by numerical simulation without consuming time, materials, and labor effort. The analyzed results keep consistent with the practical welding process. From the above discussion, the proposed method is acceptable and beneficial for guiding the practical production.

Acknowledgments This research has been supported by the National Natural Science Foundation of China (NSFC) under Grant No. 51323009, the National Basic Research Program (973 Program) of China under Grant No. 2014CB046703, and the National Natural Science Foundation of China (NSFC) under Grant No. 51505163 and 51421062. The authors also would like to thank the anonymous referees for their valuable comments.

References

1. Benyounis KY, Olabi AG (2008) Optimization of different welding processes using statistical and numerical approaches—a reference guide. Adv Eng Soft 39(6):483–496. doi:10.1016/j.advengsoft.2007.03.012
2. Casalino G, Mortello M, Peyre P (2015b) Yb–YAG laser offset welding of AA5754 and T40 butt joint. J Mater Process Tech 223:139–149. doi:10.1016/j.jmatprotec.2015.04.003
3. Leo P, Renna G, Casalino G, Olabi AG (2015) Effect of power distribution on the weld quality during hybrid laser welding of an Al–Mg alloy. Opt Laser Technol 73:118–126. doi:10.1016/j.optlastec.2015.04.021
4. Casalino G, Mortello M, Campanelli SL (2015a) Ytterbium fiber laser welding of Ti6Al4V alloy. J Manuf Process 20:250–256. doi:10.1016/j.jmapro.2015.07.003
5. Zhang YL, FG L, Cui HC, Cai Y, Guo ST, Tang XH (2016) Investigation on the effects of parameters on hot cracking and tensile shear strength of overlap joint in laser welding dissimilar Al alloys. Int J Adv Manuf Tech:1–10. doi:10.1007/s00170-016-8383-0
6. Fukuda S, Morita H, Yamauchi Y, Nagasawa I, Tsuji S (1990) Expert system for determine welding condition for a pressure vessel. ISIJ Int 30:150–154. doi:10.2355/isijinternational.30.150
7. Dhas JER, Kumanan S (2011) Optimization of parameters of submerged arc weld using non conventional techniques. Appl Soft Comput 11(8):5198–5204. doi:10.1016/j.asoc.2011.05.041
8. Qin GL, Meng XM, BL F (2015) High speed tandem gas tungsten arc welding process of thin stainless steel plate. J Mater Process Tech 220:58–64. doi:10.1016/j.jmatprotec.2015.01.011
9. Tarng YS, Yang WH (1998) Optimisation of the weld bead geometry in gas tungsten arc welding by the Taguchi method. Int J Adv Manuf Tech 14(8):549–554. doi:10.1007/BF01301698
10. Casalino G, Curcio F, Minutolo FMC (2005) Investigation on Ti6Al4V laser welding using statistical and Taguchi approaches. J Mater Process Tech 167(2):422–428. doi:10.1016/j.jmatprotec.2005.05.031
11. Datta S, Bandyopadhyay A, Pal PK (2008) Application of Taguchi philosophy for parametric optimization of bead geometry and HAZ width in submerged arc welding using a mixture of fresh flux and fused flux. Int J Adv Manuf Tech 36(7):689–698. doi:10.1007/s00170-006-0894-7
12. Vijayan S, Raju R, Subbaiah K, Sridhar N, Rao SRK (2010a) Friction stir welding of Al–Mg alloy optimization of process parameters using Taguchi method. Exp Techniques 34(5):37–44. doi:10.1111/j.1747-1567.2009.00563.x
13. Koilraj M, Sundareswaran V, Vijayan S, Koteswara RSR (2012) Friction stir welding of dissimilar aluminum alloys AA2219 to AA5083—optimization of process parameters using Taguchi technique. Mater Design 42:1–7. doi:10.1016/j.matdes.2012.02.016
14. Correia DS, Gonçalves CV, Junior SSC, Ferraresi VA (2004) GMAW welding optimization using genetic algorithms. J Braz Soc Mech Sci 26(1):28–32. doi:10.1590/S1678-58782004000100005
15. Winiczenko R (2016) Effect of friction welding parameters on the tensile strength and microstructural properties of dissimilar AISI 1020-ASTM A536 joints. Int J Adv Manuf Tech 84(5):941–955. doi:10.1007/s00170-015-7751-5
16. Mackwood AP, Crafer RC (2005) Thermal modelling of laser welding and related processes: a literature review. Opt Laser Technol 37(2):99–115. doi:10.1016/j.optlastec.2004.02.017
17. Belhadj A, Bessrour J, Masse JE, Bouhafs M, Barrallier L (2010) Finite element simulation of magnesium alloys laser beam welding. J Mater Process Tech 210(9):1131–1137. doi:10.1016/j.jmatprotec.2010.02.023
18. Wang H, Shi YW, Gong SL (2006) Numerical simulation of laser keyhole welding processes based on control volume methods. J Phys D Appl Phys 39(21). doi:10.1088/0022-3727/39/21/032
19. Franco A, Romoli L, Musacchio A (2014) Modelling for predicting seam geometry in laser beam welding of stainless steel. Int J Therm Sci 79:194–205. doi:10.1016/j.ijthermalsci.2014.01.003
20. Vijayan S, Raju R, Rao SRK (2010b) Multiobjective optimization of friction stir welding process parameters on aluminum alloy AA 5083 using Taguchi-based grey relation analysis. Mater Manuf Process 25(11):1206–1212. doi:10.1080/10426910903536782
21. Sathiya P, Jaleel MYA, Katherasan D, Shanmugarajan B (2011) Optimization of laser butt welding parameters with multiple performance characteristics. Opt Laser Technol 43(3):660–673. doi:10.1016/j.optlastec.2010.09.007
22. Olabi AG, Casalino G, Benyounis KY, Hashmi MSJ (2006) An ANN and Taguchi algorithms integrated approach to the optimization of CO2 laser welding. Adv Eng Softw 37(10):643–648. doi:10.1016/j.advengsoft.2006.02.002
23. Tarng YS, Juang SC, Chang CH (2002) The use of grey-based Taguchi methods to determine submerged arc welding process parameters in hardfacing. J Mater Process Tech 128(1):1–6. doi:10.1016/S0924-0136(01)01261-4
24. Ai YW, Shao XY, Jiang P, Li PG, Liu Y, Yue C (2015) Process modeling and parameter optimization using radial basis function neural network and genetic algorithm for laser welding of dissimilar materials. Appl Phys A-Mater 121(2):555–569. doi:10.1007/s00339-015-9408-5
25. Ducharme R, Williams K, Kapadia P, Dowden J, Steen B, Glowacki M (1994) The laser welding of thin metal sheets: an integrated keyhole and weld pool model with supporting experiments. J Phys D Appl Phys 27(8). doi:10.1088/0022-3727/27/8/006
26. Xia PY, Yan F, Kong FR, Wang CM, Liu JH, XY H, Pang SY (2014) Prediction of weld shape for fiber laser keyhole welding based on finite element analysis. Int J Adv Manuf Tech 75(1):363–372. doi:10.1007/s00170-014-6129-4
27. Goldak J, Chakravarti A, Bibby M (1984) A new finite element model for welding heat sources. Metall Mater Trans B Process Metall Mater Process Sci 15(2):299–305. doi:10.1007/BF02667333
28. Nguyen Q, Yang C (2015) Inverse determination of laser power on laser welding with a given width penetration by a modified Newton–Raphson method. Int Commun Heat Mass 65:15–21. doi:10.1016/j.icheatmasstransfer.2015.04.003
29. Sebestova H, Havelkova M, Chmelickova H (2014) Energy losses estimation during pulsed-laser seam welding. Metall Mater Trans B Process Metall Mater Process Sci 45(3):1116–1121. doi:10.1007/s11663-014-0029-8

30. Benyounis KY, Olabi AG, Hashmi MSJ (2005) Effect of laser welding parameters on the heat input and weld-bead profile. J Mater Process Tech 164:978–985. doi:10.1016/j.jmatprotec.2005.02.060
31. Reisgen U, Schleser M, Mokrov O, Ahmed E (2012) Statistical modeling of laser welding of DP/TRIP steel sheets. Opt Laser Technol 44(1):92–101. doi:10.1016/j.optlastec.2011.05.025
32. Casalino G, Campanelli SL, Ludovico AD (2013) Laser-arc hybrid welding of wrought to selective laser molten stainless steel. Int J Adv Manuf Tech 68(1–4):209–216. doi:10.1007/s00170-012-4721-z
33. Chukkan JR, Vasudevan M, Muthukumaran S, Kumar RR, Chandrasekhar N (2015) Simulation of laser butt welding of AISI 316 L stainless steel sheet using various heat sources and experimental validation. J Mater Process Tech 219:48–59. doi:10.1016/j.jmatprotec.2014.12.008
34. Guan YC, Zhou W, Zheng HY, Hong MH, Zhu Y, Qi BJ (2015) Effect of pulse duration on heat transfer and solidification development in laser-melt magnesium alloy. Appl Phys A-Mater 119(5):437–442. doi:10.1007/s00339-015-9105-4